New insights into multiyear La Nina dynamics from the perspective of a near-annual ocean process

F. Y. Liu, W. J. Zhang, F. F. Jin, F. Jiang, Julien Boucharel, S. Q. Hua

New Insights into Multiyear La Niña Dynamics from the Perspective of a Near-Annual Ocean Process

FANGYU LIU,[a] WENJUN ZHANG,[a] FEI-FEI JIN,[b] FENG JIANG,[a,c] JULIEN BOUCHAREL,[b,c] AND SUQIONG HU[a]

[a] *CIC-FEMD/ILCEC, Key Laboratory of Meteorological Disaster of Ministry of Education (KLME), Nanjing University of Information Science and Technology, Nanjing, China*
[b] *Department of Atmospheric Sciences, School of Ocean and Earth Science and Technology (SOEST), University of Hawai'i at Mānoa, Honolulu, Hawaii*
[c] *University of Toulouse, LEGOS, IRD, Toulouse, France*

(Manuscript received 6 July 2022, in final form 14 June 2023, accepted 20 July 2023)

ABSTRACT: El Niño–Southern Oscillation (ENSO) exhibits highly asymmetric temporal evolutions between its warm and cold phases. While El Niño events usually terminate rapidly after their mature phase and show an already established transition into the cold phase by the following summer, many La Niña events tend to persist throughout the second year and even reintensify in the ensuing winter. While many mechanisms were proposed, no consensus has been reached yet and the essential physical processes responsible for the multiyear behavior of La Niña remain to be illustrated. Here, we show that a unique ocean physical process operates during multiyear La Niña events. It is characterized by rapid double reversals of zonal ocean current anomalies in the equatorial Pacific and exhibits a fairly regular near-annual periodicity. Mixed-layer heat budget analyses reveal comparable contributions of the thermocline and zonal advective feedbacks to the SST anomaly growth in the first year of multiyear La Niña events; however, the zonal advective feedback plays a dominant role in the reintensification of La Niña events. Furthermore, the unique ocean process is identified to be closely associated with the preconditioning heat content state in the central to eastern equatorial Pacific before the first year of La Niña, which has been shown in previous studies to play an active role in setting the stage for the future reintensification of La Niña. Despite systematic underestimation, the above oceanic process can be broadly reproduced by state-of-the-art climate models, providing a potential additional source of predictability for the multiyear La Niña events.

KEYWORDS: Asymmetry; ENSO; Ocean dynamics; Tropical variability

1. Introduction

El Niño–Southern Oscillation (ENSO) features anomalous large-scale sea surface temperature (SST) warming in the central-eastern equatorial Pacific along with coupled changes in atmospheric circulations (e.g., Rasmusson and Carpenter 1982; Neelin et al. 1998; Wallace et al. 1998), both of which exert profound impacts on worldwide weather and socioeconomics (Cashin et al. 2017; McPhaden et al. 2020). Since it is the most pronounced mode of global interannual climate variability, fundamental ENSO theories have long been proposed to comprehend its oscillatory behavior, such as the coupled ocean–atmosphere instability (Bjerknes 1969) and delayed negative feedbacks (e.g., Schopf and Suarez 1988; Battisti and Hirst 1989; Jin 1997a,b; Picaut et al. 1997). While explaining the overall development and phase transition of ENSO events, these models, however, cannot offer further insights into several ENSO asymmetric behaviors, such as in amplitude, spatial patterns, atmospheric teleconnections, and climate impacts (e.g., Deser and Wallace 1987; Hoerling et al. 1997; Burgers and Stephenson 1999; Kang and Kug 2002; Yu and Liu 2003; An and Jin 2004; An 2008; Zhang et al. 2009; Zhang and Jin 2012). ENSO events also exhibit a distinct asymmetry in their temporal evolution with the warm phase being typically limited to 1 year and the cold phase frequently lasting longer (e.g., Kessler 2002; Ohba and Ueda 2009; Okumura and Deser 2010; McGregor et al. 2012; Choi et al. 2013; DiNezio and Deser 2014; Hu et al. 2017; Wu et al. 2019). Specifically, El Niño and La Niña events develop in boreal spring and summer and peak toward the end of the calendar year. After its mature phase, El Niño events tend to terminate rapidly by the next summer, whereas La Niña events often persist throughout the second year and even reintensify during the subsequent winter. Multiyear La Niña events are known to strongly affect summertime rainfall in southern Asia and Africa (Archer et al. 2017; Raj Deepak et al. 2019; Anderson et al. 2023) and pose a threat of persistent droughts in western Asia and South America (Barlow et al. 2002; Hoerling and Kumar 2003; Okumura et al. 2017).

A considerable literature has developed around the possible mechanisms of ENSO's evolution asymmetry. One potential process is the nonlinear atmospheric response to SST anomalies between El Niño and La Niña events (e.g., Ohba and Ueda 2009; Wu et al. 2010; McGregor et al. 2012; Choi et al. 2013; Dommenget et al. 2013; Chen et al. 2016). In contrast to La Niña events, the equatorial precipitation and wind anomalies are shifted eastward during El Niño events, due to the nonlinear SST–convection relationship and the warm west–cold east climatological SST distribution (Hoerling et al. 1997;

Supplemental information related to this paper is available at the Journals Online website: https://doi.org/10.1175/JCLI-D-22-0505.s1.

Corresponding author: Wenjun Zhang, zhangwj@nuist.edu.cn

DOI: 10.1175/JCLI-D-22-0505.1

TABLE 1. List of CMIP6 models with the length of simulation, numbers of single-year and multiyear La Niña events and phase-locking characteristics for pi-Control simulations. Asterisks indicate that models meet the criteria.

No.	Model name	Length of simulation (years)	No. of single-year events	No. of multiyear events	Phase locking
1	ACCESS-CM2*	500	120	15	Yes
2	ACCESS-ESM1-5	900	182	30	Yes
3	AWI-CM-1-1-MR	500	—	—	No
4	BCC-CSM2-MR*	600	141	14	Yes
5	CAMS-CSM1-0*	500	107	28	Yes
6	CanESM5-CanOE	501	—	—	No
7	CanESM5	1000	—	—	No
8	CESM2-FV2	500	82	34	Yes
9	CESM2*	1200	159	87	Yes
10	CESM2-WACCM-FV2*	500	81	34	Yes
11	CESM2-WACCM	499	63	32	Yes
12	CNRM-CM6-1	500	89	31	Yes
13	CNRM-ESM2-1	500	104	24	Yes
14	E3SM-1-0*	500	74	35	Yes
15	E3SM-1-1-ECA	251	—	—	No
16	EC-Earth3-LR*	201	29	10	Yes
17	EC-Earth3	501	64	40	Yes
18	EC-Earth3-Veg-LR*	501	77	28	Yes
19	EC-Earth3-Veg*	500	86	33	Yes
20	FGOALS-f3-L	500	—	—	No
21	GFDL-CM4*	500	57	44	Yes
22	GISS-E2-1-G	851	—	—	No
23	GISS-E2-1-H	801	—	—	No
24	HadGEM3-GC31-LL*	500	68	34	Yes
25	HadGEM3-GC31-MM*	500	64	42	Yes
26	IITM-ESM	200	34	15	Yes
27	INM-CM4-8	531	—	—	No
28	INM-CM5-0	1201	—	—	No
29	IPSL-CM6A-LR	2000	—	—	No
30	MCM-UA-1-0	500	—	—	No
31	MIROC6	800	56	55	Yes
32	MIROC-ES2L	500	25	47	Yes
33	MPI-ESM-1-2-HAM	780	—	—	No
34	MPI-ESM1-2-HR	500	—	—	No
35	MPI-ESM1-2-LR	1000	—	—	No
36	MRI-ESM2-0*	701	94	55	Yes
37	NESM3	500	—	—	No
38	NorESM2-LM	501	64	27	Yes
39	NorESM2-MM	500	60	31	Yes
40	SAM0-UNICON*	700	68	63	Yes

Ohba and Ueda 2009). Therefore, the associated surface wind anomalies in the western Pacific are relatively weak and more affected by the remote forcing from the Indian Ocean during El Niño (e.g., Ohba and Ueda 2007; Okumura and Deser 2010; Okumura et al. 2011). The asymmetric zonal wind anomalies in the western Pacific can contribute to different evolutions between El Niño and La Niña through changes in eastward oceanic Kelvin waves features and associated SST response in the central-eastern Pacific. In addition, the asymmetric wind stress curl strength favors the development of a long-term discharge of the equatorial Pacific, increasing the likelihood of a transition from El Niño to La Niña events rather than vice versa (Neske et al. 2021). The much stronger southward shift of central Pacific wind anomalies observed during El Niño than La Niña events is another asymmetric atmospheric response (e.g., Harrison 1987; Harrison and Larkin 1998; McGregor et al. 2012; Stuecker et al. 2013; Zhang et al. 2015) that accelerates the discharge of equatorial heat content and contributes to rapid El Niño transition but plays a minor role in the persistence of negative SST anomalies in the equatorial Pacific during La Niña events (e.g., Harrison and Vecchi 1999; McGregor et al. 2012, 2013).

In addition to the nonlinear atmospheric responses, ENSO-related oceanic processes also exhibit a highly asymmetric response to atmospheric wind anomalies (e.g., DiNezio and Deser 2014; Hu et al. 2014, 2017; An and Kim 2017). As one of the main processes for ENSO transition, the delayed thermocline feedback (i.e., the delayed adjustment of thermocline to wind anomalies) is more effective in terminating El Niño than La Niña events, arising from both the stronger wind response to SST anomalies and the stronger mixed-layer temperature adjustment to the thermocline depth during warm

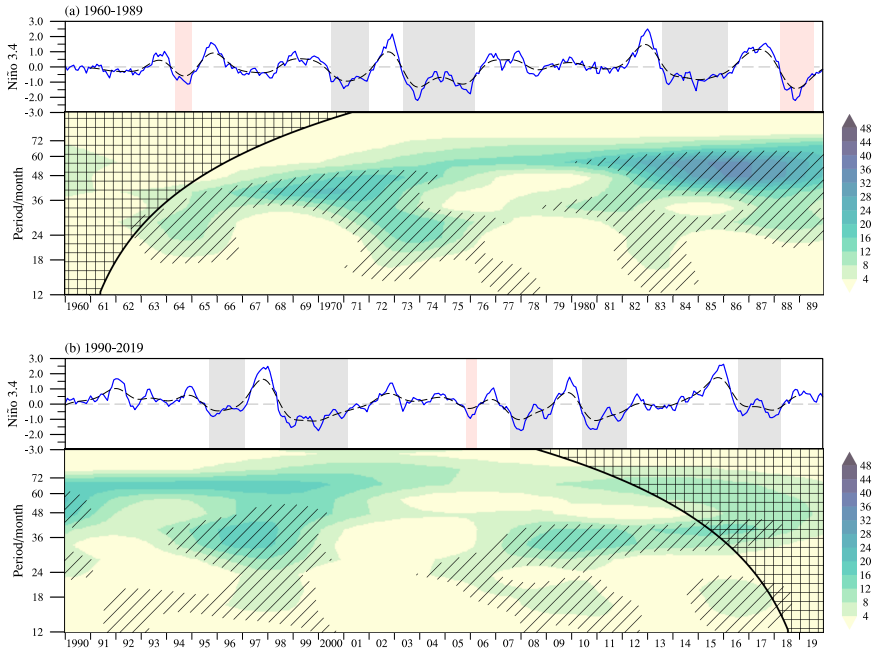

FIG. 1. Time series of the Niño-3.4 indices and associated Morlet wavelet spectrum during (a) 1960–89 and (b) 1990–2019. Blue solid and black dashed lines indicate raw and 24-month low-pass filtered Niño-3.4 indices, respectively. Multiyear and single-year La Niña events are shaded in light gray and pink, respectively. The wavelet spectrum shows the amplitude as a function of oscillation period and time, with the values above the 95% confidence level hatched.

phases (DiNezio and Deser 2014). The larger and more susceptible response of oceanic waves to winds during El Niño than La Niña events is also emphasized by trapping more atmospheric momentum via a shallower thermocline in the western Pacific (An and Kim 2017). Due to the slower and weaker recharge process during La Niña, the large discharge of ocean heat content associated with strong El Niño events in the preceding year cannot be restored by a single-year La Niña event, which further promotes the reoccurrence of La Niña in the second year (Iwakiri and Watanabe 2021). Besides those nonlinear processes in the tropical Pacific, capacitor effects from other tropical oceans (e.g., Kug et al. 2006; Frauen and Dommenget 2012; Dommenget and Yu 2017; An and Kim 2018; Cai et al. 2019; Wang 2019; Chikamoto et al. 2020; Wang and Wang 2021) and teleconnections from the extratropical Pacific (Kim and Yu 2020; Park et al. 2021) were also suggested to explain the asymmetry of ENSO evolution. In particular, multiyear La Niña events tend to have a wide meridional structure and are well connected with the preceding negative phase of the Pacific meridional mode (PMM), which may lead to an inefficient recharge process and contribute to the persistence of La Niña (Park et al. 2021).

Despite these several mechanisms proposed to explain the asymmetry between El Niño and La Niña evolutions, the essential physical conditions responsible for the multiyear behavior of La Niña deserve further attention. Different from El Niño events exhibiting relatively regular evolutions, La Niña events display a wide diversity in their evolutions. Some La Niña events present a typical single-year evolution analogous to El Niño, whereas some other events show a long persistence with a multiyear evolution. Previous studies argued that the multiyear La Niña events could be linked to the amplitude of preceding warm events (e.g., Hu et al. 2014; Wu et al. 2019; Iwakiri and Watanabe 2021). However, some moderate El Niño events such as the 1994/95, 2006/07, and 2009/10 events, are also followed by multiyear La Niña events. Therefore, more effort is still needed to understand the substantial dynamics controlling the duration and behavior of La Niña events. Rather than elucidating their triggering mechanisms, this study focuses on diagnosing the distinct dynamical oceanic processes at work during multiyear La Niña events in both observations and state-of-the-art global coupled climate models.

The rest of the paper is organized as follows. Section 2 presents the datasets and methods. Unique oceanic processes associated with multiyear La Niña events are discussed in section 3, and some dynamical analyses are presented in section 4. Section 5 reports on possible oceanic preconditions for the reintensification of La Niña. Section 6 presents the simulation of multiyear La Niña in the phase 6 of the Coupled Model Intercomparison Project (CMIP6) preindustrial control (pi-Control) experiments. Finally, the main conclusions are summarized and discussed in section 7.

2. Data and methodology

a. Data and methodology

To examine the observed La Niña evolution, we use the monthly SST product from the Hadley Centre sea ice and SST

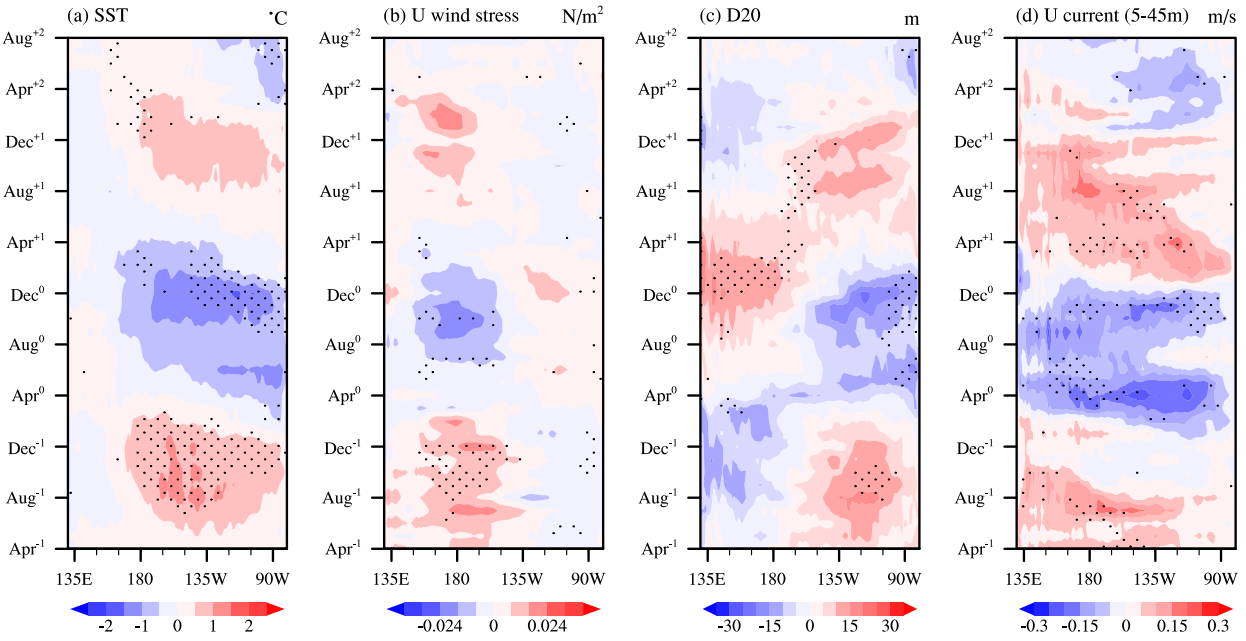

FIG. 2. Time–longitude Hovmöller diagrams of anomalous (a) SST (°C), (b) zonal wind stress (N m^{-2}), (c) D20 (m), and (d) surface zonal current (5–45 m average; m s^{-1}) averaged within 5°S–5°N for the single-year La Niña events composite. Stippling represents values above the 95% confidence level.

dataset (HadISST) version 1.1 (Rayner et al. 2003) and surface wind stress, ocean temperature, and horizontal currents from the European Centre for Medium-Range Weather Forecasts (ECMWF) reanalysis (ORAS5; Zuo et al. 2019). In addition, other atmospheric and oceanic reanalysis datasets are also used for verification including horizontal momentum flux from the National Centers for Environmental Prediction (NCEP-2; Kanamitsu et al. 2002) and ocean temperature and horizontal currents from the NCEP Global Ocean Data Assimilation System (GODAS; Saha et al. 2006). The main conclusions remain the same when using NCEP-2 or GODAS (see Figs. S1–S8 in the online supplemental material). The ORAS5 and GODAS data

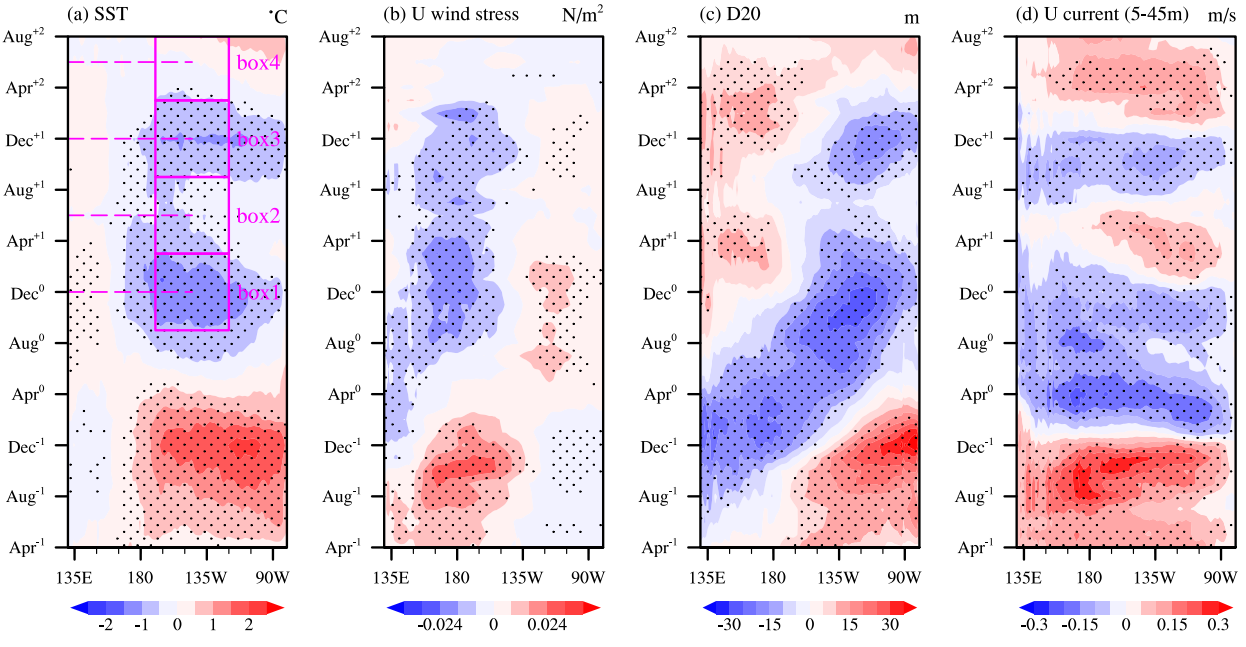

FIG. 3. As in Fig. 2, but for the composite of multiyear La Niña events. The region highlighted by pink boxes are utilized for defining "warm conditions" and "cold conditions."

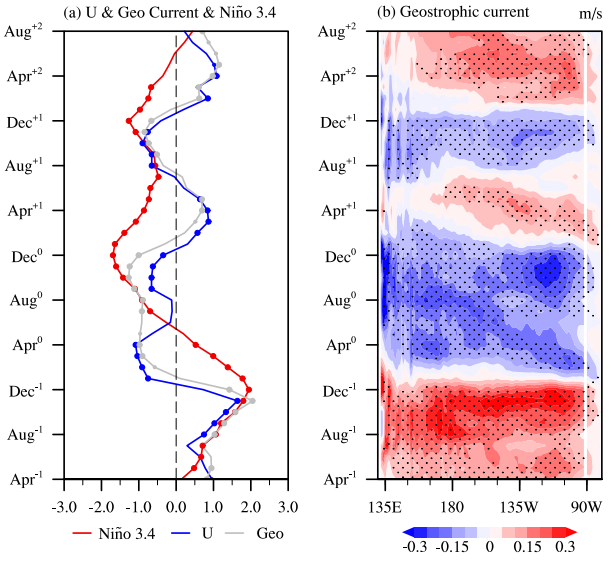

FIG. 4. (a) Normalized composite evolution of the Niño-3.4 index (red line), surface zonal current anomalies (averaged within 2°S–2°N, 100°–170°W; blue line), and geostrophic current anomalies (averaged in the same region; gray line) for the multiyear La Niña events. Small and big dots represent the values exceeding the 90% and 95% confidence levels, respectively. (b) Time–longitude Hovmöller diagram of anomalous geostrophic current (m s^{-1}) averaged within 2°S–2°N for the multiyear La Niña events. Stippling represents values above the 95% confidence level.

are available for the periods of 1958 to the present and 1980 to the present, respectively. Based on the subsurface ocean temperature data, the thermocline depth (D20) is roughly measured as the depth of the 20°C isotherm, a common proxy for the tropical Pacific. Our analyses cover the period from 1960 to 2019, and anomalies for all the variables are computed as the departures from a monthly climatology over the entire study period. All the datasets are nondetrended, and the qualitative results remain unchanged when trends are removed. The statistical significance tests are performed using a two-tailed Student's *t* test.

In addition, to evaluate the multiyear behavior of La Niña events in climate models, we analyze the pi-Control simulations of 40 models (see Table 1) from CMIP6 (Eyring et al. 2016). Monthly outputs of SST, ocean temperature, and horizontal currents are used over the entire available time period of each model. All anomalies are computed with respect to a monthly mean climatology derived from the overall respective period of each product/model.

b. *Definition of single-year and multiyear La Niña events*

Following previous studies (e.g., Okumura et al. 2017; Wu et al. 2019), La Niña events were identified when the 3-month running-mean Niño-3.4 index (SST anomalies averaged in the domain 5°S–5°N, 120°–170°W) is below minus three-quarters of the standard deviation in any month from October^{0} to February^{+1}, with years −1, 0, +1, and +2 denoting the preceding year of La Niña, La Niña developing year, La Niña decaying year, and the next year, respectively; the months of these years are shown as month^{-1}, month^{0}, month^{+1}, and month^{+2}. La Niña events were then categorized into single-year or multiyear events if the Niño-3.4 index is above or below respectively minus half of the standard deviation in any month during October^{+1}–February^{+2}. The relatively smaller threshold is used for the second year considering that the second peak is commonly weaker than the first peak. Three single-year La Niña cases (1964/65, 1988/89, and 2005/06) and eight multiyear La Niña cases (1970–72, 1973–76, 1983–85, 1995–97, 1998–2001, 2007–09, 2010–12, and 2016–18) can be identified in both HadISST and ORAS5 based on this definition. We also identified single-year and multiyear

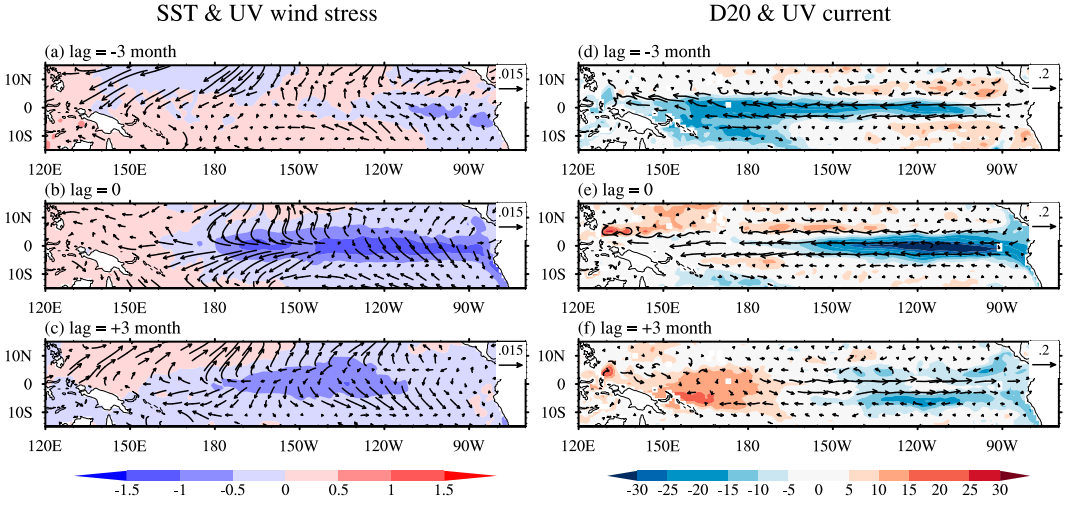

FIG. 5. Composite differences of SST (shading; °C) and zonal wind stress (vectors; N m^{-2}) anomalies between cold and warm conditions at (a) 3 months before the mature phase, (b) the mature phase, and (c) 3 months after the mature phase. (d)–(f) As in (a)–(c), but for composite difference of D20 (shading; m) and horizontal surface current anomalies (vectors; m s^{-1}).

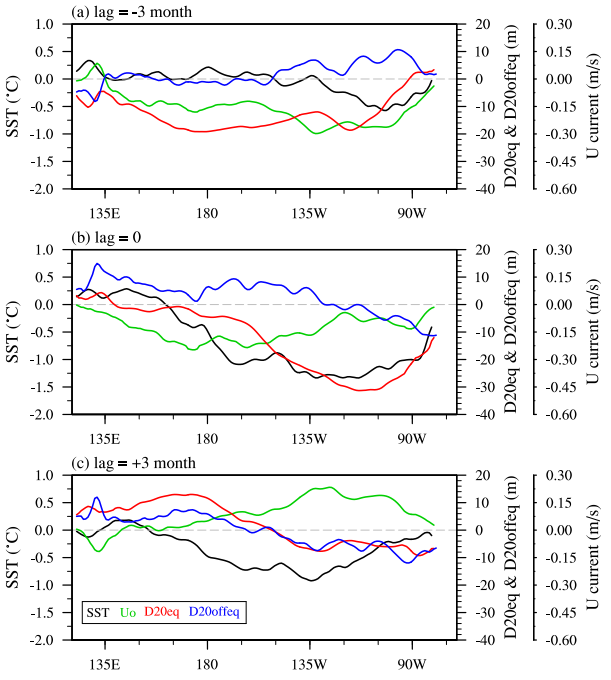

FIG. 6. Composite differences of SST anomalies (within 2°S–2°N; black line), zonal current anomalies (within 2°S–2°N; green line), equatorial D20 anomalies (within 2°S–2°N; red line) and off-equatorial D20 anomalies (within 4°–8°N; blue line) between warm and cold conditions at (a) 3 months before the mature phase, (b) the mature phase, and (c) 3 months after the mature phase. All the indices are smoothed out based on a 5°C running window.

La Niña events in climate models according to the above definition.

3. Unique ocean processes associated with multiyear La Niña events

ENSO is an interannual climate oscillation, exhibiting a dominant periodicity spanning 2–4 years before 2000, and 2–3 years after 2000 due to a regime shift in its spatial structure (Zhang et al. 2019) and nonlinearity (Boucharel et al. 2009). Besides this change in ENSO's dominant periodicity, the Morlet wavelet spectrum of the Niño-3.4 index reveals prominent short-term fluctuations in some discrete periods at near-annual time scales (12–24 months) (see also Jin et al. 2003; Kang et al. 2004). This near-annual mode seems to be predominantly active during cold ENSO phases and in particular during multiyear La Niña events rather than single-year events (Fig. 1). This encourages us to investigate the role of a potential deterministic ocean process operating on these time scales in the multiyear behavior of some La Niña events.

To do so, we first show the time evolution of anomalous SST, zonal wind, D20, and zonal current for single-year and multiyear La Niña events composites in Figs. 2 and 3, respectively. During the winter preceding the single-year La Niña, weakly positive SST anomalies emerge over the central and eastern Pacific (Fig. 2a). In the subsequent months, as a result of the easterly wind anomalies over the far western Pacific around April^{0} (Fig. 2b), the shoaling of the equatorial thermocline propagates eastward and contributes to the anomalous cooling in the eastern Pacific (Fig. 2c). La Niña thereby develops through air–sea interactions between the easterly wind anomalies and SST cooling (Figs. 2a,c). Simultaneously, the westward oceanic current anomalies driven by strengthened easterly winds also act to reinforce the cooling in the central-eastern Pacific via the advection of the eastern equatorial Pacific's cold waters (Fig. 2d). It is clear that the classic recharging process via the Sverdrup transport (Jin 1997a,b) leads to the rapid demise of these two single-year La Niña events after their peak.

In contrast, multiyear La Niña events, which feature a similar evolution to the single-year La Niña events prior to the first winter peak, exhibit totally different characteristics of their subsequent air–sea evolution. In contrast to the rapid disappearance of the single-year events, the negative SST anomalies of the multiyear events persist into the boreal spring of the second year and intensify again in the following winter (Fig. 3a). Accordingly, the anomalous easterlies prevail over the central-western Pacific and the thermocline depth anomalies in the eastern Pacific basically remain of the same sign throughout year^{+1} (Figs. 3b,c). However, this persistence is not found in the zonal current characteristics. Unlike for single-year La Niña events, the zonal current shows fairly regular oscillations during multiyear La Niña events with a near annual periodicity from August^{0} to August^{+2} (Fig. 3d). The first reversal of the zonal currents from negative to positive values around December^{0} can be observed in both the single-year and multiyear La Niña events. The anomalous eastward currents during March^{+1}–June^{+1} (Fig. 3d) correspond to weakened La Niña–related SST anomalies (Fig. 3a). The eastward zonal current anomalies do not terminate La Niña event, possibly due to the strong thermocline shoaling (DiNezio and Deser 2014) or persistent easterly wind anomalies over the western Pacific (Wu et al. 2019). The evident inconsistency between the zonal current and wind anomalies around April^{+1} indicates that the equatorial current during this period is not locally wind forced. As shown in Fig. 4, the anomalous surface current is indeed dominated by the geostrophic current rather than the Ekman current, indicating the importance of equatorial oceanic Kelvin and Rossby waves in controlling the zonal current variation.

To extract and quantify further this fast vacillation, we first define two "cold conditions" (Fig. 3a, boxes 1 and 3) and two relatively "warm conditions" (Fig. 3a, boxes 2 and 4) based on the composite SSTA evolution of multiyear La Niña events. Boxes 1 and 3 denote the first and second peak phases of multiyear La Niña respectively, and boxes 2 and 4 denote the first and second transition stages respectively. On this basis, December^{0} and December^{+1} are defined as two mature phases of the cold conditions, September^{0} and September^{+1} as the 3-month lead phases of cold conditions, and March^{+1} and March^{+2} as the 3-month lag phases of cold conditions. Similar definitions are also conducted on warm conditions. Then we conduct the difference of these three phases between the so-called cold conditions and warm conditions to highlight the evolution of this fast vacillation as follows.

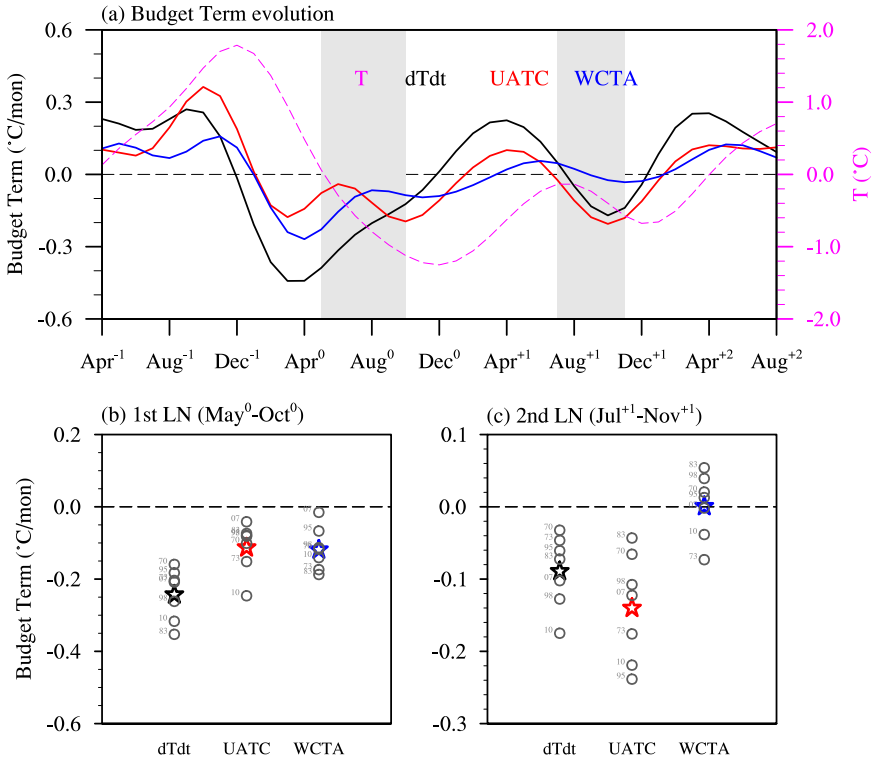

FIG. 7. (a) Temporal evolutions of the key composite terms of the mixed layer heat budget for multiyear La Niña events, averaged over the Niño-3.4 region. Each term in the figure denotes the mixed layer temperature anomaly (T; magenta line) and its tendency (dT/dt; black line), the advection of mean temperature by anomalous zonal current (UATC; red line) and the advection of anomalous temperature by mean vertical current (WCTA; blue line). The developing phases of the first (May^0–October^0) and second (July^{+1}–November^{+1}) developing year for multiyear La Niña events are shaded in gray. (b) Scatterplot of the key mixed layer heat budget terms averaged within the first developing year (May^0–October^0) for the five multiyear La Niña events (gray dots) and their composite (colored stars). (c) As in (b), but averaged during the second developing year (July^{+1}–November^{+1}).

$$\begin{cases} \text{3–month lead phase} : \dfrac{\text{Var(September}^0\text{)} + \text{Var(September}^{+1}\text{)}}{2} - \dfrac{\text{Var(March}^{+1}\text{)} + \text{Var(March}^{+2}\text{)}}{2} \\ \text{mature phase} \quad : \dfrac{\text{Var(December}^0\text{)} + \text{Var(December}^{+1}\text{)}}{2} - \dfrac{\text{Var(June}^{+1}\text{)} + \text{Var(June}^{+2}\text{)}}{2} \\ \text{3–month lag phse} \quad : \dfrac{\text{Var(March}^{+1}\text{)} + \text{Var(March}^{+2}\text{)}}{2} - \dfrac{\text{Var(September}^{+1}\text{)} + \text{Var(September}^{+2}\text{)}}{2} \end{cases}. \quad (1)$$

The variable Var can be specified as anomalous SST, wind stress, D20, or ocean currents.

The differences in the air–sea field composites between cold and warm conditions at three phases are displayed to highlight the evolution of this fast oscillation (Fig. 5). This method smooths out the interannual variability associated with the ENSO mode but retains the relatively high-frequency variability related to the fast vacillation. At the developing phase, slightly negative SST anomalies emerge in the eastern Pacific, with weak easterly anomalies confined in the far eastern Pacific (Fig. 5a). The obvious westward current anomalies along with cold equatorial subsurface temperature anomalies favor the development of negative SST anomalies (Fig. 5d). During the mature phase, cold SST anomalies are strengthened and expanded from the equatorial eastern Pacific into the central Pacific through advection processes, along with strong easterly anomalies over the equatorial western Pacific (Figs. 5b,e). During the decaying phase, the anomalous zonal current unexpectedly reverses and the basin-wide thermocline deepens along the equator, especially in the western Pacific (Fig. 5f). The anomalous warm advection by the

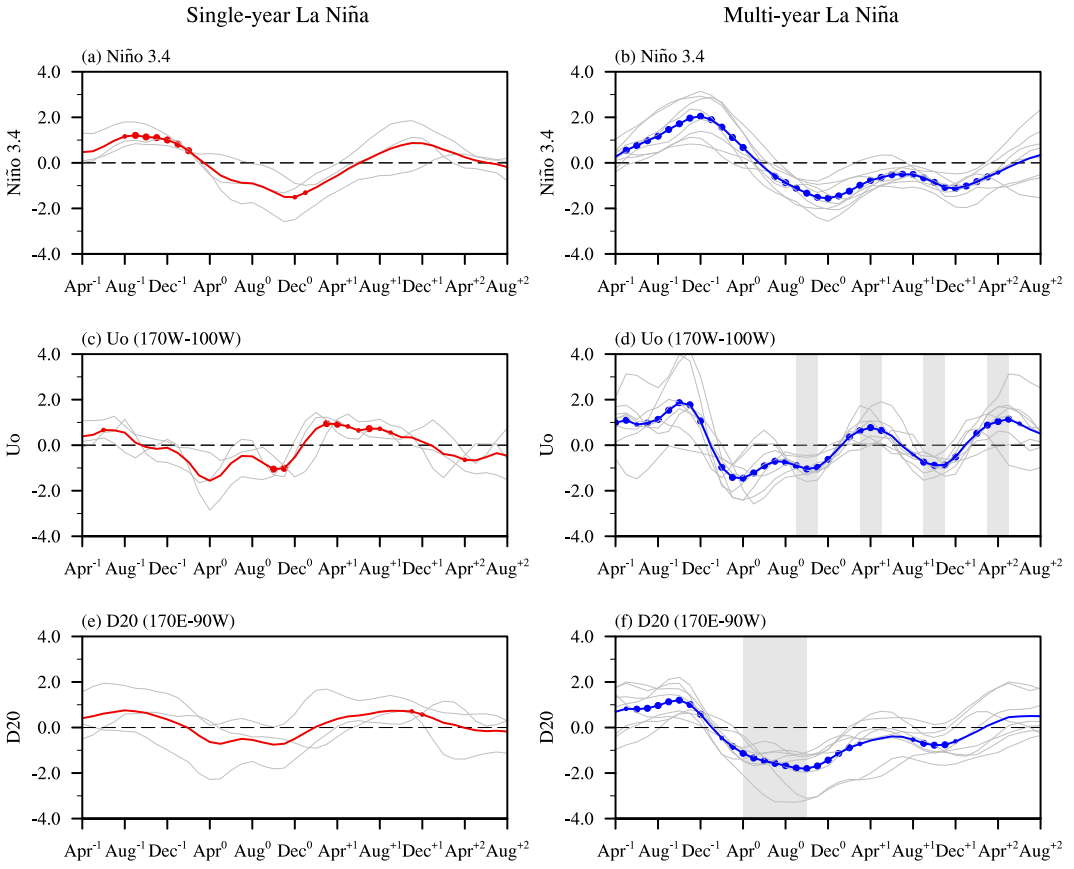

FIG. 8. Normalized temporal evolution of the Niño-3.4 indices for (a) single-year and (b) multiyear La Niña events. (c),(d) and (e),(f) As in (a) and (b), but for Uo indices (equatorial zonal current averaged within 5°S–5°N, 100°–170°W) and D20 indices (D20 averaged within 5°S–5°N, 170°E–90°W), respectively. The time series for individual and composite events are shown by thin gray and thick colored curves, respectively. The gray shaded areas in (d) and (f) indicate the stages for defining the Uo_MLN index and D20 indicator, respectively. Small and big dots represent the values exceeding the 90% and 95% confidence levels, respectively.

eastward zonal current weakens the cold SST anomalies effectively and promotes the transition from cold to warm conditions (Fig. 5c).

This rapid variability is also evident in variations of the thermocline depth over the equator and off the equator (Fig. 6). From the developing to peak phase, the negative equatorial thermocline depth anomalies, indicating the upwelling Kelvin waves, propagate eastward toward the eastern Pacific (Figs. 6a,b). Accompanied by the strengthening and westward extension of cold SST anomalies, off-equatorial downwelling Rossby waves develop to the west of the cooling, and upwelling Rossby waves develop to the east at the mature phase (Figs. 6a,b). These Rossby waves contribute significantly to the distribution of anomalous zonal geostrophic currents. During the transition phase, the off-equatorial downwelling Rossby waves are reflected into equatorial downwelling Kelvin waves at the western boundary, which propagate rapidly eastward and promote to the reversal of the zonal current anomalies (Fig. 6c). Thus, the rapidly reversed equatorial surface current anomalies are associated with oceanic Kelvin and Rossby waves.

4. Dynamical processes controlling the multiyear La Niña events

To illustrate the predominant dynamical processes associated with the multiyear La Niña events, we now conduct a heat budget analysis on the mixed-layer ocean temperature of the equatorial Pacific based on the ORAS5 data. The anomalous heat budget equation can be written following previous studies (An and Jin 2004):

$$\frac{\partial T_a}{\partial t} = -U_c\frac{\partial T_a}{\partial x} - U_a\frac{\partial T_c}{\partial x} - U_a\frac{\partial T_a}{\partial x} - V_c\frac{\partial T_a}{\partial y} - V_a\frac{\partial T_c}{\partial y} - V_a\frac{\partial T_a}{\partial y} - W_c\frac{\partial T_a}{\partial z} - W_a\frac{\partial T_c}{\partial z} - W_a\frac{\partial T_a}{\partial z} + \frac{Q_a}{\rho_0 C_p H} + R. \quad (2)$$

Here, the subscripts c and a denote the climatological mean and corresponding anomalies, respectively. The term T represents the mixed layer temperature and u, v, and w represent the

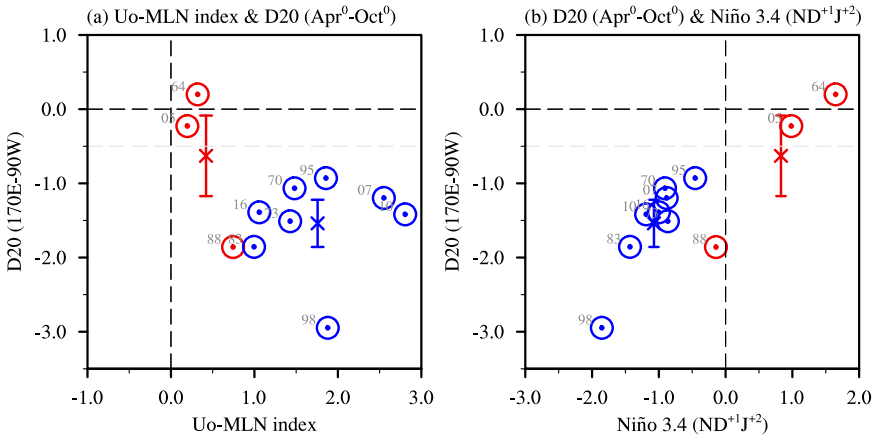

FIG. 9. Scatterplot of the normalized (a) D20 indicator as a function of the Uo-MLN index, (b) D20 indicator as a function of the second-year amplitude which is measured as the winter (ND^{+1}J^{+2}) Niño-3.4 index. Red and blue circles denote the single-year and multiyear La Niña events, respectively. Colored crosses denote composites and the error bars represent one standard deviation among multiyear La Niña events.

three-dimensional mixed layer ocean currents. The variable Q denotes the ocean net heat flux including the shortwave, longwave, sensible, and latent heat flux. The terms ρ and C_p are the density (=1025 kg m^{-3}) and heat capacity of the seawater (=3989.24 J kg^{-1} K^{-1}), respectively, and H is the mixed layer (=45 m). The qualitative conclusions remain unchanged if we use other depths, such as 50 and 60 m. The last term R is the residual term that includes contributions associated with the diffusion, entrainment, and subgrid-scale processes. To focus on the contribution of the main processes on the interannual time scale, we have here performed a bandpass filtering of 6–84 months in the heat budget analyses. All the budget terms are averaged over the Niño-3.4 region, and the qualitative results remain unchanged when we use other regions, such as the Niño-3 region (Fig. S10) or Niño-4 region (Fig. S11).

The two major processes of ENSO dynamics, namely the zonal advection of the mean temperature by the anomalous current ($U_a\partial T_c/\partial x$) and the vertical advection of the anomalous temperature by the mean upwelling ($W_c\partial T_a/\partial z$), are displayed here to assess their relative contributions to the temperature tendency (Fig. 7). It has long been known that the two terms, referred to as zonal advective and thermocline feedbacks respectively, are largely responsible for the growth and phase transitions of ENSO (Jin and An 1999). However, these two terms play distinct roles in the first and second years of multiyear La Niña events. During the first year, the thermocline and zonal advective feedbacks make comparable contributions to the development of SST cooling in the central and eastern equatorial Pacific (Fig. 7a). In contrast to the first year, the reintensification of La Niña events in the second year is mainly attributed to the zonal advective feedback, with little contribution from the thermocline feedback (Fig. 7a). The difference of relative roles for the two key feedbacks on the temperature tendency is further evidenced by the results from a composite analysis during the first and second developing stages (Figs. 7b,c), hinting at different dynamics responsible for the first and second years of multiyear La Niña events. It is possibly related to the westward shift of the SST anomalies associated with the unique ocean processes (Fig. 5), which favors the zonal advective over the thermocline feedback because of a relatively weak climatological upwelling in the west compared to the east.

5. Possible oceanic precondition for the reintensification of La Niña

The above analyses have revealed the occurrence of a unique oceanic process at work during multiyear La Niña events characterized by two rapid reversals of zonal ocean current anomalies and westward propagation of SST anomalies. To further explore the different oceanic processes between the single-year and multiyear La Niña events, we show in Fig. 8 the evolutions of the Niño-3.4 index, anomalous zonal current in the eastern Pacific (averaged within 5°S–5°N, 100°–170°W), and anomalous D20 in the central-eastern Pacific (averaged within 5°S–5°N, 170°E–90°W). Consistent with Figs. 2 and 3, the single-year La Niña events rapidly decay in the following boreal spring; however, the negative SST anomalies can persist through the second year (Figs. 8a,b). Accordingly, distinct oceanic processes could play important roles in their SST anomaly evolutions (Figs. 8c,d). Despite many differences in the D20 evolution, neither of the three single-year La Niña events displays a typical discharge–recharge process (Fig. 8e). In contrast, the large discharge state during the developing phase is pronounced during the first year of multiyear La Niña events (Fig. 8f). The observations show that a much stronger discharge state appears to occur in the central and eastern equatorial Pacific for multiyear La Niña than for single-year La Niña, which has been mentioned in previous studies (DiNezio and Deser 2014; Hu et al. 2014; Wu et al. 2019; Iwakiri and Watanabe 2021). Therefore, the D20 condition during the La Niña developing phase from April^0 to October^0 (gray shading in Fig. 8f) could

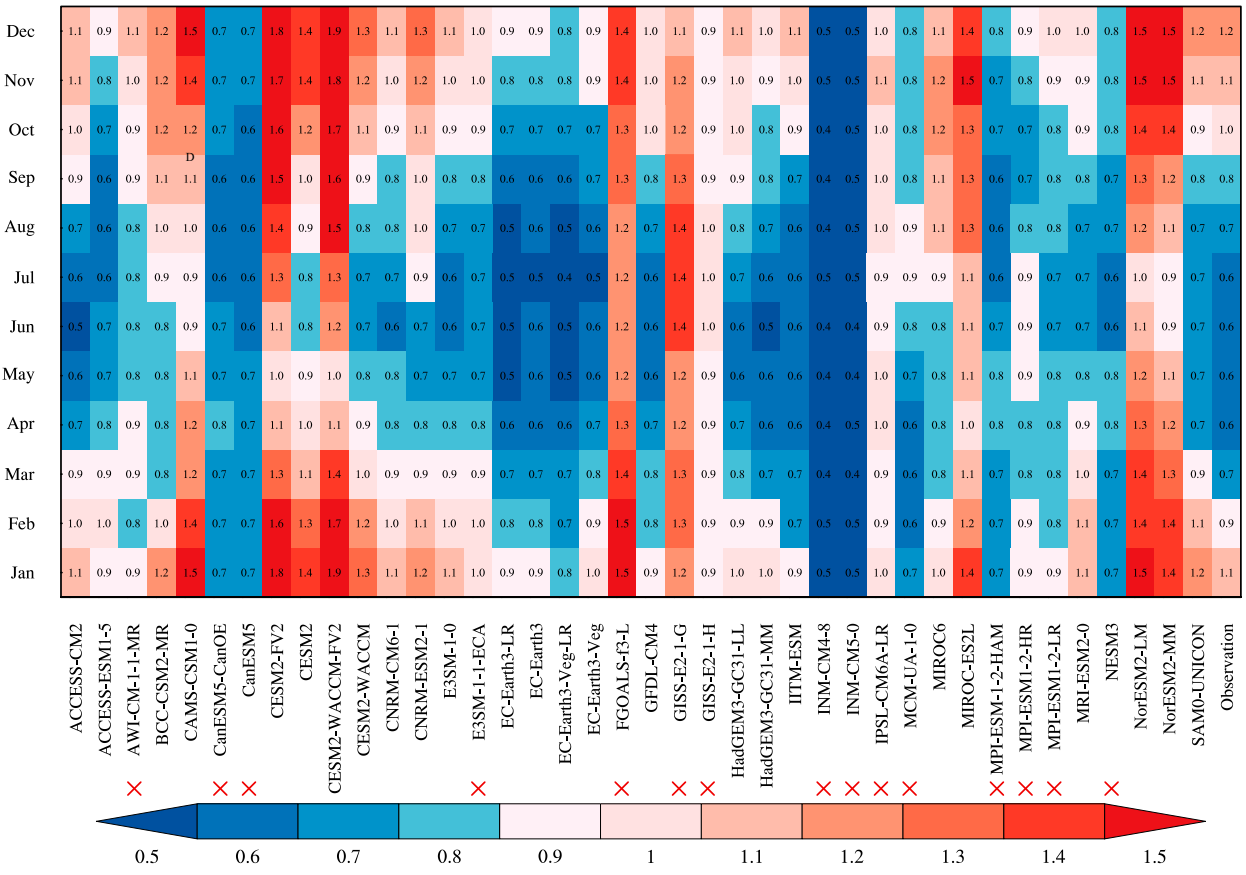

FIG. 10. Portrait diagram of the standard deviation in terms of all the years of Niño3.4 indices simulated by the CMIP6 models compared to observations (arranged in columns, with the observation displayed in the last column). Red crosses indicate that the models do not meet the phase-locking criterion.

be identified as one possible precondition for the emergence of double-dip La Niña events.

As previously established, the double-dip La Niña events are also characterized by processes related to the rapid shift in zonal surface circulation. To quantify the multiyear La Niña events' temporal behavior based on the evolution of regionally averaged zonal current in the central-eastern equatorial Pacific, we define the Uo_MLN index to capture the main features of the 5°S–5°N, 100°–170°W [Uo] as

$$\text{Uo\_MLN} = \frac{(U_2 + U_4)}{2} - \frac{(U_1 + U_3)}{2}, \tag{3}$$

where U_1, U_2, U_3, and U_4 represent [Uo] at the first negative phase, first positive phase, second negative phase, and second positive phase, respectively (gray shading in Fig. 8d). The Uo_MLN index, representing the amplitude of the unique oceanic process with twice reversals of zonal current anomalies, well distinguishes the multiyear La Niña events from the single-year events (Fig. 9a). Most multiyear La Niña events are accompanied by relatively strong Uo_MLN indices, while the Uo_MLN index is relatively weak for single-year La Niña events (Fig. 9a), suggesting that strong discharge state favors the occurrence of this unique ocean process during multiyear La Niña events. It is noted that the 1988/89 single-year La Niña case displays a strong discharge state, yet fails to reintensify in the next winter. Actually, the unique oceanic process associated with multiyear La Niña appears to be at play during this single-year La Niña event (Figs. S9c,d). However, it is found that the multiyear behavior of SST anomalies is strongly hindered by the unexpectedly active westerlies over the far western equatorial Pacific since October^{+1} (Fig. S9b), which was mentioned in the previous study by Hu et al. (2014) as a trigger for downwelling Kelvin waves that may have hampered the reintensification of negative SST anomalies. Also, the easterly wind anomalies are weaker around summer^{+1} (Fig. S9b) than those of the composite multiyear La Niña (Fig. 3b), which could also affect the evolution of this event. The connection between the preconditioning D20 state and the Niño-3.4 index during the second winter (ND^{+1}J^{+2}) is further examined in Fig. 9b. There appears to be a highly negative linear correlation (R = 0.86, statistically significant at the 95% confidence level), suggesting that the multiyear behavior of La Niña is closely related to the discharge condition in the developing phase of the first year. Again, these results suggest that the preconditioning heat content state in the central to eastern equatorial Pacific could provide a potential source of predictability for the emergence of reintensification of La Niña events.

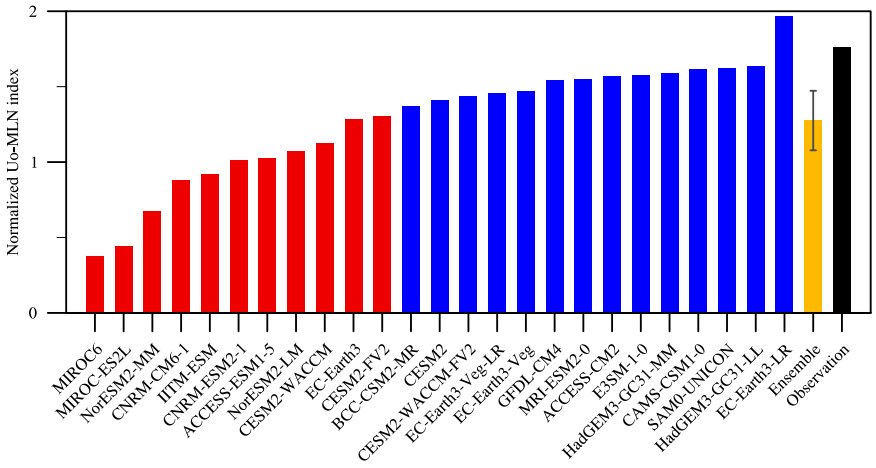

FIG. 11. The normalized Uo-MLN indices of multiyear La Niña events for 25 CMIP6 models and observations as a reference. Models are ranked by the Uo-MLN indices in an ascending order, with "better" and "worse" performing models indicated by blue and red bars, respectively. The error bar for the multimodel ensemble mean corresponds to one standard deviation.

6. Simulation of multiyear La Niña in CMIP6 pi-Control experiments

Considering the limited sample size of the short observational record, we further investigate the above ocean processes during the multiyear La Niña events as simulated in the preindustrial (pi-Control) experiments of 14 CMIP6 models. These 14 models are selected from 40 CMIP6 models (Table 1) based on two criteria: the correct ENSO phase-locking feature and the realistically simulated unique ocean processes associated with the multiyear La Niña. On the one hand, these models should simulate the phase-locking phenomenon of ENSO realistically, which can be measured by the monthly standard deviation of the Niño-3.4 index (Fig. 10). Observations show that ENSO's preferred peak months tend to occur at the end of the calendar year from September to February, with the standard deviation of Niño-3.4 ranging from 0.6 to 1.2. Therefore, only models with an ENSO peak locked to the fall–winter season (September–February) and a ratio between the maximum and minimum standard deviation of Niño-3.4 above 1.5 (i.e., 0.75 times the observation) are considered. Among the 40 models, 15 marked with crosses in Fig. 10 do not reach the criterion and are thereby excluded. On the other hand, the observed oceanic dynamics associated with multiyear La Niña should also be realistically captured by the models. As shown in Fig. 11, there are systematic model biases in the simulation of the unique oceanic process associated with multiyear La Niña events. We further identified 14 models (blue bars in Fig. 11) in which the simulated normalized Uo-MLN indices are above 1.32 standard deviation (i.e., 0.75 times the observation). Besides, almost all the models show a much smaller ratio of multiyear La Niña to single-year La Niña in the CMIP6 simulations relative to the observations. The discrepancy between the model simulation and the observation could be due to the systematic bias in simulated ENSO complexity in climate models (Iwakiri and Watanabe 2021) and the uncertainties in estimating the ratio based on the limited observational record (Wittenberg 2009; Deser et al. 2017).

The temporal evolution of anomalous SST and zonal currents for the composite of multiyear La Niña events is shown for the 14 selected models (Fig. 12). These relatively "better" performing models realistically capture the two rapid reversals of zonal current anomalies during the multiyear La Niña events. In fact, other models also have the ability to simulate the rapid reversals of zonal currents despite a weak amplitude (Fig. S12), except for the MIROC6 and MIROC-ES2L models. We found that almost all the selected models exhibit a stronger discharge state during the developing phase of the first year for the multiyear La Niña events compared to the single-year events (Fig. 13), which is consistent with the observation. Nevertheless, the marked difference in discharge state between single-year and multiyear La Niña events is strongly underestimated in the models. The preconditioning discharge state does not seem to be the only factor controlling the amplitude of the second year for the multiyear La Niña events (Table S1), and other mechanisms (Hu et al. 2014; Luo et al. 2017; Wu et al. 2019; Kim and Yu 2020; Park et al. 2021) may also play a role in the reintensification of La Niña, which requires further investigation.

7. Conclusions and discussion

In the present study, the evolution characteristics and associated oceanic dynamical processes for multiyear La Niña events are investigated in observational datasets and CMIP6 model simulations. The multiyear La Niña events show a pronounced near-annual periodicity in the equatorial Pacific SST, featuring two reversals of the zonal current anomalies. In contrast, this unique ocean process is remarkably absent during single-year La Niña events except for the 1988/89 event. The zonal advective and thermocline feedbacks make comparable contributions to the La Niña development during the first year. However, the zonal advective feedback plays a dominant role in the reintensification of the multiyear La Niña

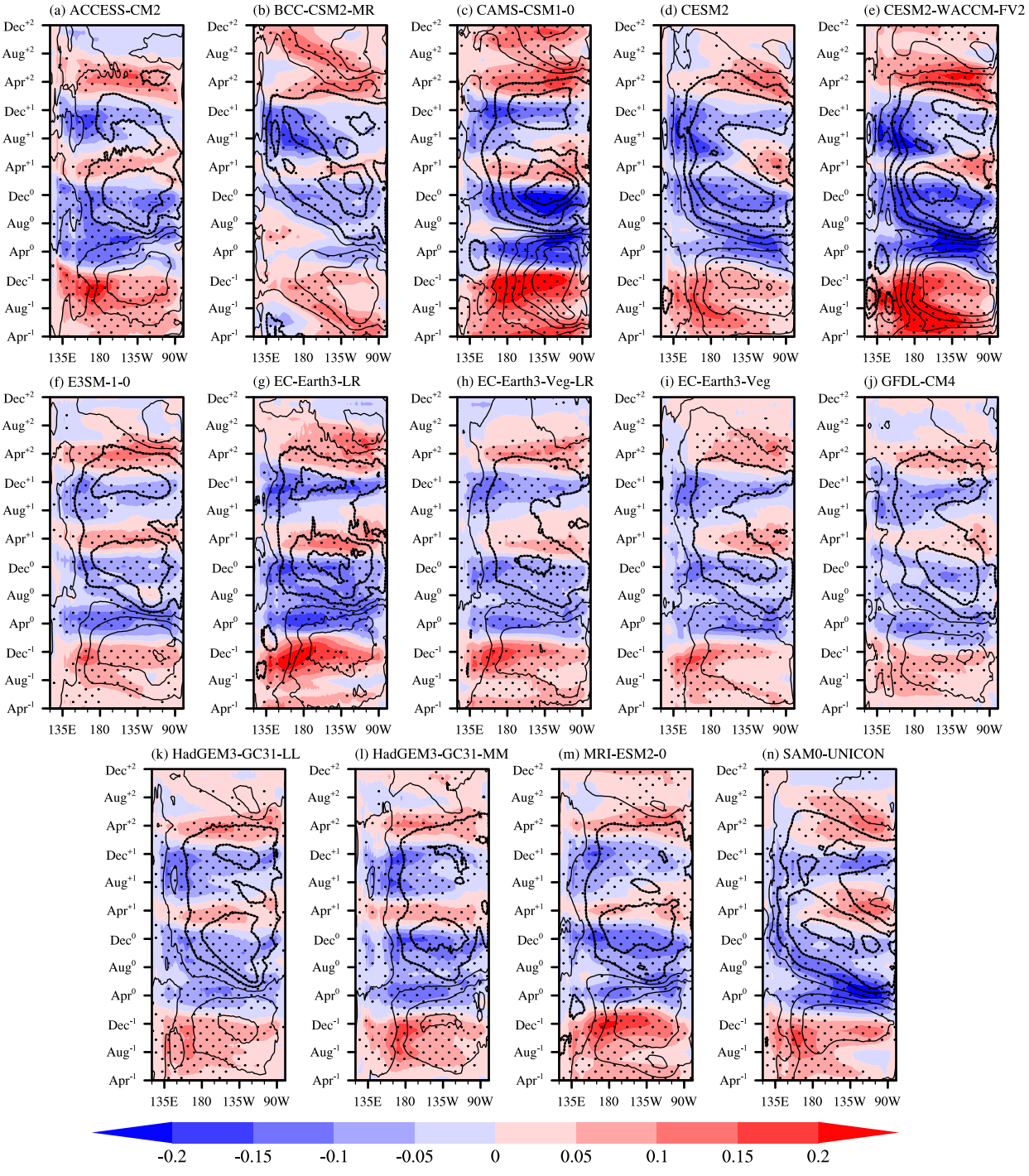

FIG. 12. Time–longitude Hovmöller diagrams of anomalous SST (contours with an interval of 0.5°C; solid and dashed for positive and negative values, respectively) and surface zonal current (shading; m s^{-1}) averaged in the equatorial band (5°S–5°N) for the multiyear La Niña events composites from 14 "better"-performing CMIP6 models. Stippling represents the zonal current values above the 95% confidence level.

events, related to the westward expanded SST anomaly center. As stated by previous studies (DiNezio and Deser 2014; Hu et al. 2014; Wu et al. 2019; Iwakiri and Watanabe 2021), the strong discharge state acts to favor the generation of multiyear La Niña events in the following years. Here we demonstrate that the discharge condition during the developing stage (April^0–October^0) can well distinguish the subsequent single- and multiyear La Niña events, and could be identified as a potential

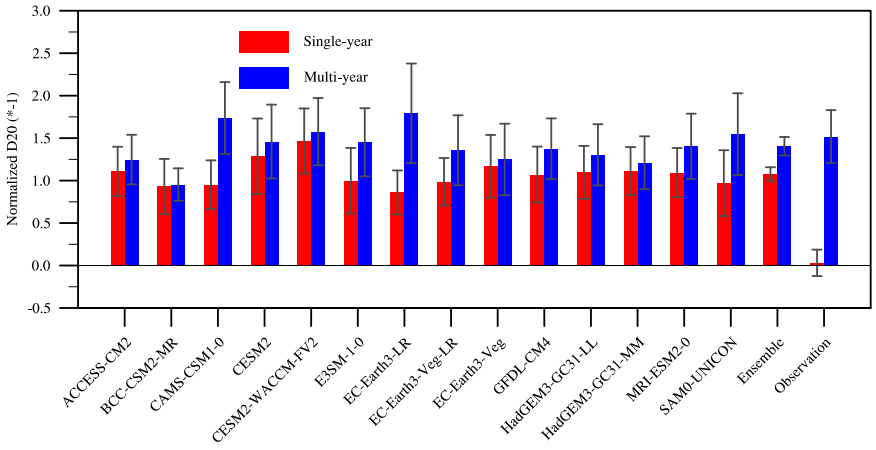

FIG. 13. The normalized D20 indicators of single-year (red bars) and multiyear (blue bars) La Niña events for 14 "better"-performing models and their ensemble mean. The observational composite is also displayed in the last column for comparison. The error bars represent one standard deviation error.

precursor for the emergence of the double-dip La Niña events. In our manuscript, we present evidence that the majority of CMIP6 models that realistically simulate the near-annual zonal advective process can reasonably capture the reintensification of La Niña events. In contrast, models lacking this process fail to reproduce the occurrence of double La Niña events. This suggests that this unique oceanic process is of paramount importance for the dynamics of multiyear La Niña events.

The primary goal of this study was not to elucidate the precise triggering mechanisms behind multiyear La Niña events. Rather, we identified distinct oceanic processes during these prolonged La Niña events. While the triggering mechanism for multiyear La Niña occurrence events still remains controversial, it is widely accepted that the preceding discharged state could set the stage for the reintensification of La Niña events. Previous studies have proposed a strong link between a high recharged rate and the amplitude of El Niño events (Hu et al. 2014; Wu et al. 2019; Iwakiri and Watanabe 2021). However, except for the case of the 1997/98 super El Niño, the discharged states of the other three super El Niño events (1972/73, 1982/83, 2015/16) do not appear to differ from those of moderate events (1969/70, 1994/95, 2006/07, 2009/10). In addition, the midlatitude climate variability may also play a role in influencing the recharge–discharge process in the tropical Pacific (Park et al. 2021). Previous research also suggests that the Indian and Atlantic Oceans may also have remote effects on the initiation and maintenance of ENSO events through interbasin interactions (Kug et al. 2006; Ohba and Ueda 2007; Okumura and Deser 2010; Frauen and Dommenget 2012; Dommenget and Yu 2017; Cai et al. 2019; Wang 2019; Chikamoto et al. 2020; Wang and Wang 2021). These tropical basin interactions seem to have played a key role in particular for maintaining the recent prolonged 2020–22 La Niña event (Hasan et al. 2022).

In addition, a few El Niño events also appear to persist for more than a year. For example, the 1986–88 El Niño event lasted for 18 months according to the Climate Prediction Center's definition. However, we found that the unique ocean process during multiyear La Niña is not detected during this particular warm event (not shown). It further highlights the peculiarity of the multiyear La Niña events, which might be related to the instability induced by the strong east–west oceanic temperature gradient in the tropical Pacific. At present the exact reasons for the unique ocean process to occur in cold rather than warm ENSO phases are not clear and require further investigation.

Acknowledgments. This work was supported by the National Key R&D Program of China (2022YFF0801602) and the National Nature Science Foundation of China (42088101). FL was funded through the Postgraduate Research and Practice Innovation Program of Jiangsu Province (KYCX21_0968). JB is funded through the French Agence Nationale de la Recherche project Make Our Planet Great Again MOPGA "Trocodyn" (ANR-17-MPGA-0018) and the Région Occitanie.

Data availability statement. The data that support the findings of this study are available from the following resources:

- https://www.metoffice.gov.uk/hadobs/hadisst/data/download.html
- https://www.ecmwf.int/en/forecasts/dataset/ocean-reanalysis-system-5
- https://psl.noaa.gov/data/gridded/data.ncep.reanalysis2.html
- https://www.psl.noaa.gov/data/gridded/data.godas.html
- https://esgf-node.llnl.gov/search/cmip6/

REFERENCES

An, S.-I., 2008: Interannual variations of the tropical ocean instability wave and ENSO. *J. Climate*, **21**, 3680–3686, https://doi.org/10.1175/2008JCLI1701.1.

——, and F.-F. Jin, 2004: Nonlinearity and asymmetry of ENSO. *J. Climate*, **17**, 2399–2412, https://doi.org/10.1175/1520-0442(2004)017<2399:NAAOE>2.0.CO;2.

——, and J.-W. Kim, 2017: Role of nonlinear ocean dynamic response to wind on the asymmetrical transition of El Niño and La Niña. *Geophys. Res. Lett.*, **44**, 393–400, https://doi.org/10.1002/2016GL071971.

——, and ——, 2018: ENSO transition asymmetry: Internal and external causes and intermodel diversity. *Geophys. Res. Lett.*, **45**, 5095–5104, https://doi.org/10.1029/2018GL078476.

Anderson, W., B. I. Cook, K. Slinski, K. Schwarzwald, A. McNally, and C. Funk, 2023: Multiyear La Niña events and multiseason drought in the Horn of Africa. *J. Hydrometeor.*, **24**, 119–131, https://doi.org/10.1175/JHM-D-22-0043.1.

Archer, E. R. M., W. A. Landman, M. A. Tadross, J. Malherbe, H. Weepener, P. Maluleke, and F. M. Marumbwa, 2017: Understanding the evolution of the 2014–2016 summer rainfall seasons in southern Africa: Key lessons. *Climate Risk Manage.*, **16**, 22–28, https://doi.org/10.1016/j.crm.2017.03.006.

Barlow, M., H. Cullen, and B. Lyon, 2002: Drought in central and Southwest Asia: La Niña, the warm pool, and Indian Ocean precipitation. *J. Climate*, **15**, 697–700, https://doi.org/10.1175/1520-0442(2002)015<0697:DICASA>2.0.CO;2.

Battisti, D. S., and A. C. Hirst, 1989: Interannual variability in a tropical atmosphere–ocean model: Influence of the basic state, ocean geometry and nonlinearity. *J. Atmos. Sci.*, **46**, 1687–1712, https://doi.org/10.1175/1520-0469(1989)046<1687:IVIATA>2.0.CO;2.

Bjerknes, J., 1969: Atmospheric teleconnections from the equatorial Pacific. *Mon. Wea. Rev.*, **97**, 163–172, https://doi.org/10.1175/1520-0493(1969)097<0163:ATFTEP>2.3.CO;2.

Boucharel, J., B. Dewitte, B. Garel, and Y. du Penhoat, 2009: ENSO's non-stationary and non-Gaussian character: The role of climate shifts. *Nonlinear Processes Geophys.*, **16**, 453–473, https://doi.org/10.5194/npg-16-453-2009.

Burgers, G., and D. B. Stephenson, 1999: The "normality" of El Niño. *Geophys. Res. Lett.*, **26**, 1027–1030, https://doi.org/10.1029/1999GL900161.

Cai, W., and Coauthors, 2019: Pantropical climate interactions. *Science*, **363**, eaav4236, https://doi.org/10.1126/science.aav4236.

Cashin, P., K. Mohaddes, and M. Raissi, 2017: Fair weather or foul? The macroeconomic effects of El Niño. *J. Int. Econ.*, **106**, 37–54, https://doi.org/10.1016/j.jinteco.2017.01.010.

Chen, M., T. Li, X. Shen, and B. Wu, 2016: Relative roles of dynamic and thermodynamic processes in causing evolution asymmetry between El Niño and La Niña. *J. Climate*, **29**, 2201–2220, https://doi.org/10.1175/JCLI-D-15-0547.1.

Chikamoto, Y., Z. F. Johnson, S.-Y. S. Wang, M. J. McPhaden, and T. Mochizuki, 2020: El Niño–Southern Oscillation evolution modulated by Atlantic forcing. *J. Geophys. Res. Oceans*, **125**, e2020JC016318, https://doi.org/10.1029/2020JC016318.

Choi, K.-Y., G. A. Vecchi, and A. T. Wittenberg, 2013: ENSO transition, duration, and amplitude asymmetries: Role of the nonlinear wind stress coupling in a conceptual model. *J. Climate*, **26**, 9462–9476, https://doi.org/10.1175/JCLI-D-13-00045.1.

Deser, C., and J. M. Wallace, 1987: El Niño events and their relation to the Southern Oscillation: 1925–1986. *J. Geophys. Res.*, **92**, 14 189–14 196, https://doi.org/10.1029/JC092iC13p14189.

——, I. R. Simpson, K. A. McKinnon, and A. S. Phillips, 2017: The Northern Hemisphere extratropical atmospheric circulation response to ENSO: How well do we know it and how do we evaluate models accordingly? *J. Climate*, **30**, 5059–5082, https://doi.org/10.1175/JCLI-D-16-0844.1.

DiNezio, P. N., and C. Deser, 2014: Nonlinear controls on the persistence of La Niña. *J. Climate*, **27**, 7335–7355, https://doi.org/10.1175/JCLI-D-14-00033.1.

Dommenget, D., and Y. Yu, 2017: The effects of remote SST forcings on ENSO dynamics, variability and diversity. *Climate Dyn.*, **49**, 2605–2624, https://doi.org/10.1007/s00382-016-3472-1.

——, T. Bayr, and C. Frauen, 2013: Analysis of the non-linearity in the pattern and time evolution of El Niño Southern Oscillation. *Climate Dyn.*, **40**, 2825–2847, https://doi.org/10.1007/s00382-012-1475-0.

Eyring, V., S. Bony, G. A. Meehl, C. A. Senior, B. Stevens, R. J. Stouffer, and K. E. Taylor, 2016: Overview of the Coupled Model Intercomparison Project phase 6 (CMIP6) experimental design and organization. *Geosci. Model Dev.*, **9**, 1937–1958, https://doi.org/10.5194/gmd-9-1937-2016.

Frauen, C., and D. Dommenget, 2012: Influences of the tropical Indian and Atlantic Oceans on the predictability of ENSO. *Geophys. Res. Lett.*, **39**, L02706, https://doi.org/10.1029/2011GL050520.

Harrison, D. E., 1987: Monthly mean island surface winds in the central tropical Pacific and El Niño events. *Mon. Wea. Rev.*, **115**, 3133–3145, https://doi.org/10.1175/1520-0493(1987)115<3133:MMISWI>2.0.CO;2.

——, and N. K. Larkin, 1998: El Niño–Southern Oscillation sea surface temperature and wind anomalies, 1946–1993. *Rev. Geophys.*, **36**, 353–399, https://doi.org/10.1029/98RG00715.

——, and G. A. Vecchi, 1999: On the termination of El Niño. *Geophys. Res. Lett.*, **26**, 1593–1596, https://doi.org/10.1029/1999GL900316.

Hasan, N. A., Y. Chikamoto, and M. J. McPhaden, 2022: The influence of tropical basin interactions on the 2020–2022 double-dip La Niña. *Front. Climate*, **4**, 1001174, https://doi.org/10.3389/fclim.2022.1001174.

Hoerling, M. P., and A. Kumar, 2003: The perfect ocean for drought. *Science*, **299**, 691–694, https://doi.org/10.1126/science.1079053.

——, ——, and M. Zhong, 1997: El Niño, La Niña, and the nonlinearity of their teleconnections. *J. Climate*, **10**, 1769–1786, https://doi.org/10.1175/1520-0442(1997)010<1769:ENOLNA>2.0.CO;2.

Hu, Z.-Z., A. Kumar, Y. Xue, and B. Jha, 2014: Why were some La Niñas followed by another La Niña? *Climate Dyn.*, **42**, 1029–1042, https://doi.org/10.1007/s00382-013-1917-3.

——, ——, B. Huang, J. Zhu, R.-H. Zhang, and F.-F. Jin, 2017: Asymmetric evolution of El Niño and La Niña: The recharge/discharge processes and role of the off-equatorial sea surface height anomaly. *Climate Dyn.*, **49**, 2737–2748, https://doi.org/10.1007/s00382-016-3498-4.

Iwakiri, T., and M. Watanabe, 2021: Mechanisms linking multiyear La Niña with preceding strong El Niño. *Sci. Rep.*, **11**, 17465, https://doi.org/10.1038/s41598-021-96056-6.

Jin, F.-F., 1997a: An equatorial ocean recharge paradigm for ENSO. Part I: Conceptual model. *J. Atmos. Sci.*, **54**, 811–829, https://doi.org/10.1175/1520-0469(1997)054<0811:AEORPF>2.0.CO;2.

——, 1997b: An equatorial ocean recharge paradigm for ENSO. Part II: A stripped-down coupled model. *J. Atmos. Sci.*, **54**, 830–847, https://doi.org/10.1175/1520-0469(1997)054<0830:AEORPF>2.0.CO;2.

——, and S.-I. An, 1999: Thermocline and zonal advective feedbacks within the equatorial ocean recharge oscillator model for ENSO. *Geophys. Res. Lett.*, **26**, 2989–2992, https://doi.org/10.1029/1999GL002297.

——, J.-S. Kug, S.-I. An, and I.-S. Kang, 2003: A near-annual coupled ocean-atmosphere mode in the equatorial Pacific Ocean. *Geophys. Res. Lett.*, **30**, 1080, https://doi.org/10.1029/2002GL015983.

Kanamitsu, M., W. Ebisuzaki, J. Woollen, S.-K. Yang, J. J. Hnilo, M. Fiorino, and G. L. Potter, 2002: NCEP–DOE AMIP-II reanalysis (R-2). *Bull. Amer. Meteor. Soc.*, **83**, 1631–1644, https://doi.org/10.1175/BAMS-83-11-1631.

Kang, I.-S., and J.-S. Kug, 2002: El Niño and La Niña sea surface temperature anomalies: Asymmetry characteristics associated with their wind stress anomalies. *J. Geophys. Res.*, **107**, 4372, https://doi.org/10.1029/2001JD000393.

——, ——, S.-I. An, and F.-F. Jin, 2004: A near-annual Pacific Ocean basin mode. *J. Climate*, **17**, 2478–2488, https://doi.org/10.1175/1520-0442(2004)017<2478:ANPOBM>2.0.CO;2.

Kessler, W. S., 2002: Is ENSO a cycle or a series of events? *Geophys. Res. Lett.*, **29**, 2125, https://doi.org/10.1029/2002GL015924.

Kim, J.-W., and J.-Y. Yu, 2020: Understanding reintensified multiyear El Niño events. *Geophys. Res. Lett.*, **47**, e2020GL087644, https://doi.org/10.1029/2020GL087644.

Kug, J.-S., T. Li, S.-I. An, I.-S. Kang, J.-J. Luo, S. Masson, and T. Yamagata, 2006: Role of the ENSO–Indian Ocean coupling on ENSO variability in a coupled GCM. *Geophys. Res. Lett.*, **33**, L09710, https://doi.org/10.1029/2005GL024916.

Luo, J.-J., G. Liu, H. Hendon, O. Alves, and T. Yamagata, 2017: Inter-basin sources for two-year predictability of the multi-year La Niña event in 2010–2012. *Sci. Rep.*, **7**, 2276, https://doi.org/10.1038/s41598-017-01479-9.

McGregor, S., A. Timmermann, N. Schneider, M. F. Stuecker, and M. H. England, 2012: The effect of the South Pacific convergence zone on the termination of El Niño events and the meridional asymmetry of ENSO. *J. Climate*, **25**, 5566–5586, https://doi.org/10.1175/JCLI-D-11-00332.1.

——, N. Ramesh, P. Spence, M. H. England, M. J. McPhaden, and A. Santoso, 2013: Meridional movement of wind anomalies during ENSO events and their role in event termination. *Geophys. Res. Lett.*, **40**, 749–754, https://doi.org/10.1002/grl.50136.

McPhaden, M. J., A. Santoso, and W. Cai, 2020: Introduction to El Niño Southern Oscillation in a changing climate. *El Niño Southern Oscillation in a Changing Climate*, Amer. Geophys. Union, 1–19, https://doi.org/10.1002/9781119548164.ch1.

Neelin, J. D., D. S. Battisti, A. C. Hirst, F.-F. Jin, Y. Wakata, T. Yamagata, and S. E. Zebiak, 1998: ENSO theory. *J. Geophys. Res.*, **103**, 14 261–14 290, https://doi.org/10.1029/97JC03424.

Neske, S., S. McGregor, M. Zeller, and D. Dommenget, 2021: Wind spatial structure triggers ENSO's oceanic warm water volume changes. *J. Climate*, **34**, 1985–1999, https://doi.org/10.1175/JCLI-D-20-0040.1.

Ohba, M., and H. Ueda, 2007: An impact of SST anomalies in the Indian Ocean in acceleration of the El Niño to La Niña transition. *J. Meteor. Soc. Japan*, **85**, 335–348, https://doi.org/10.2151/jmsj.85.335.

——, and ——, 2009: Role of nonlinear atmospheric response to SST on the asymmetric transition process of ENSO. *J. Climate*, **22**, 177–192, https://doi.org/10.1175/2008JCLI2334.1.

Okumura, Y. M., and C. Deser, 2010: Asymmetry in the duration of El Niño and La Niña. *J. Climate*, **23**, 5826–5843, https://doi.org/10.1175/2010JCLI3592.1.

——, M. Ohba, C. Deser, and H. Ueda, 2011: A proposed mechanism for the asymmetric duration of El Niño and La Niña. *J. Climate*, **24**, 3822–3829, https://doi.org/10.1175/2011JCLI3999.1.

——, P. DiNezio, and C. Deser, 2017: Evolving impacts of multi-year La Niña events on atmospheric circulation and U.S. drought. *Geophys. Res. Lett.*, **44**, 11 614–11 623, http://doi.org/10.1002/2017GL075034.

Park, J.-H., S.-I. An, J.-S. Kug, Y.-M. Yang, T. Li, and H.-S. Jo, 2021: Mid-latitude leading double-dip La Niña. *Int. J. Climatol.*, **41**, E1353–E1370, https://doi.org/10.1002/joc.6772.

Picaut, J., F. Masia, and Y. du Penhoat, 1997: An advective-reflective conceptual model for the oscillatory nature of the ENSO. *Science*, **277**, 663–666, https://doi.org/10.1126/science.277.5326.663.

Raj Deepak, S. N., J. S. Chowdary, A. R. Dandi, G. Srinivas, A. Parekh, C. Gnanaseelan, and R. K. Yadav, 2019: Impact of multiyear La Niña events on the South and East Asian summer monsoon rainfall in observations and CMIP5 models. *Climate Dyn.*, **52**, 6989–7011, https://doi.org/10.1007/s00382-018-4561-0.

Rasmusson, E. M., and T. H. Carpenter, 1982: Variations in tropical sea surface temperature and surface wind fields associated with the southern oscillation/El Niño. *Mon. Wea. Rev.*, **110**, 354–384, https://doi.org/10.1175/1520-0493(1982)110<0354:VITSST>2.0.CO;2.

Rayner, N. A., D. E. Parker, E. B. Horton, C. K. Folland, L. V. Alexander, D. P. Rowell, E. C. Kent, and A. Kaplan, 2003: Global analyses of sea surface temperature, sea ice, and night marine air temperature since the late nineteenth century. *J. Geophys. Res.*, **108**, 4407, https://doi.org/10.1029/2002JD002670.

Saha, S., and Coauthors, 2006: The NCEP Climate Forecast System. *J. Climate*, **19**, 3483–3517, https://doi.org/10.1175/JCLI3812.1.

Schopf, P. S., and M. J. Suarez, 1988: Vacillations in a coupled ocean–atmosphere model. *J. Atmos. Sci.*, **45**, 549–566, https://doi.org/10.1175/1520-0469(1988)045<0549:VIACOM>2.0.CO;2.

Stuecker, M. F., A. Timmermann, F.-F. Jin, S. McGregor, and H.-L. Ren, 2013: A combination mode of the annual cycle and the El Niño/southern oscillation. *Nat. Geosci.*, **6**, 540–544, https://doi.org/10.1038/ngeo1826.

Wallace, J. M., E. M. Rasmusson, T. P. Mitchell, V. E. Kousky, E. S. Sarachik, and H. von Storch, 1998: On the structure and evolution of ENSO-related climate variability in the tropical Pacific: Lessons from TOGA. *J. Geophys. Res.*, **103**, 14 241–14 259, https://doi.org/10.1029/97JC02905.

Wang, C., 2019: Three-ocean interactions and climate variability: A review and perspective. *Climate Dyn.*, **53**, 5119–5136, https://doi.org/10.1007/s00382-019-04930-x.

Wang, J.-Z., and C. Wang, 2021: Joint boost to super El Niño from the Indian and Atlantic Oceans. *J. Climate*, **34**, 4937–4954, https://doi.org/10.1175/JCLI-D-20-0710.1.

Wittenberg, A. T., 2009: Are historical records sufficient to constrain ENSO simulations? *Geophys. Res. Lett.*, **36**, L12702, https://doi.org/10.1029/2009GL038710.

Wu, B., T. Li, and T. Zhou, 2010: Asymmetry of atmospheric circulation anomalies over the western North Pacific between El Niño and La Niña. *J. Climate*, **23**, 4807–4822, https://doi.org/10.1175/2010JCLI3222.1.

Wu, X., Y. M. Okumura, and P. N. DiNezio, 2019: What controls the duration of El Niño and La Niña events? *J. Climate*, **32**, 5941–5965, https://doi.org/10.1175/JCLI-D-18-0681.1.

Yu, J.-Y., and W. T. Liu, 2003: A linear relationship between ENSO intensity and tropical instability wave activity in the eastern Pacific Ocean. *Geophys. Res. Lett.*, **30**, 1735, https://doi.org/10.1029/2003GL017176.

Zhang, W., and F.-F. Jin, 2012: Improvements in the CMIP5 simulations of ENSO-SSTA meridional width. *Geophys. Res. Lett.*, **39**, L23704, https://doi.org/10.1029/2012GL053588.

——, J. Li, and F.-F. Jin, 2009: Spatial and temporal features of ENSO meridional scales. *Geophys. Res. Lett.*, **36**, L15605, https://doi.org/10.1029/2009GL038672.

——, H. Li, F.-F. Jin, M. F. Stuecker, A. G. Turner, and N. P. Klingaman, 2015: The annual-cycle modulation of meridional asymmetry in ENSO's atmospheric response and its dependence on ENSO zonal structure. *J. Climate*, **28**, 5795–5812, https://doi.org/10.1175/JCLI-D-14-00724.1.

——, S. Li, F. F. Jin, R. Xie, C. Liu, M. F. Stuecker, and A. Xue, 2019: ENSO regime changes responsible for decadal phase relationship variations between ENSO sea surface temperature and warm water volume. *Geophys. Res. Lett.*, **46**, 7546–7553, https://doi.org/10.1029/2019GL082943.

Zuo, H., M. A. Balmaseda, S. Tietsche, K. Mogensen, and M. Mayer, 2019: The ECMWF operational ensemble reanalysis–analysis system for ocean and sea ice: A description of the system and assessment. *Ocean Sci.*, **15**, 779–808, https://doi.org/10.5194/os-15-779-2019.